
Robust Methods for Reconstructing Brain Activity and Functional Connectivity from MEG Data

Julia P. Owen^{1,2}, David P. Wipf¹, Hagai T. Attias³, Kensuke Sekihara⁴, and Srikantan S. Nagarajan^{1,2}

¹ Biomagnetic Imaging Laboratory, Dept. Radiology and Biomedical Imaging, UCSF San Francisco, CA, USA

² Joint Graduate Group in Bioengineering UCSF/UC Berkeley, San Francisco, CA, USA

³ Golden Metallic, Inc. San Francisco, CA, USA

⁴ Dept. of Systems Design and Engineering, Tokyo Metropolitan University, Tokyo, Japan

Abstract

The synchronous brain activity measured via magnetoencephalography (MEG) arises from current dipoles located throughout the cortex. Estimating the number, location, time-course, and orientation of these dipoles, called sources, remains a challenging task, one that is significantly compounded by the effects of source correlations and interference from spontaneous brain activity and sensor noise. Likewise, assessing the interactions between the individual sources, known as *functional connectivity*, is also confounded by noise and correlations in the sensor recordings. Computational complexity has been an obstacle to computing functional connectivity. This paper demonstrates the application of an empirical Bayesian method to perform source localization with MEG data in order to estimate measures of functional connectivity. We demonstrate that brain source activity inferred from this algorithm is better suited to uncover the interactions between brain areas as compared to other commonly used source localization algorithms.

1 Introduction

Magnetoencephalography (MEG) non-invasively detects brain activity from direct measurements of the magnetic field from an array of sensors; the observed field is generated by large ensembles of neurons firing synchronously, approximated as compact current sources. Determining the combination of current sources that best explains the field recording is an ill-posed inverse problem because the number of potential sources is much greater than the number of sensors. Determining the spatial distribution, orientation, and time courses of these unknown sources is still an open inverse problem.

We have developed a novel empirical Bayesian scheme, presented in [8] and [9], that improves upon existing methods of source reconstruction in terms of reconstruction accuracy, robustness, and efficiency. The algorithm derived from this model, which we call *Champagne*, is designed to estimate the number and location of a small (sparse) set of flexible dipoles that adequately explain the observed sensor data. This method relies on having access to pre- and post-stimulus data, where the pre-stimulus data is thought to contain no stimulus-evoked brain activity. We have shown that Champagne reliably reconstructs a large number of correlated dipoles. The source time-course estimates that Champagne produces are well suited functional connectivity analyses.

Functional connectivity can be described as understanding brain function in terms of the way information is transmitted and integrated across brain networks. In the most complete case, one would like to make inferences from a causal linear model that describes the dependencies among activities across all voxels. However, due to the large number of voxels, solving such a model is computationally expensive and virtually impossible with limited, noisy data. Instead, existing techniques for estimating functional connectivity approximate the full problem in various ways, but there is a tradeoff between reducing the computational complexity and loss of sensitivity. Paradoxically, inferences about connectivity can be made from the correlations between source time-courses, but many common localization algorithms have significant trouble reconstructing correlated brain activity. Consequently, there is a fundamental problem applying many existing localization methods to functional connectivity estimation.

The solution obtained from Champagne is ideal for use in functional connectivity analyses as it is robust to highly correlated dipoles and it circumvents the issues of computational complexity by vastly pruning the number of active voxels. We present results from simulated and real MEG data showing Champagne's

efficacy in reconstructing brain activity and estimating functional connectivity as compared to standard localization techniques such as minimum variance adaptive beamforming (MVAB) [6] and sLORETA [4].

2 Methods

2.1 Source Localization: *Champagne*

The voxels time-courses (x^n) are inferred from the sensor data (y^n) using a novel source-localization algorithm called *Champagne* described in full detail in [8] and [9]. In summary, this method relies on segmenting the data into pre- and post-stimulus periods, learning the statistics of the background activity from the pre-stimulus period, and then applying the statistics of the background activity to the post-stimulus data to uncover the stimulus-evoked activity. The underlying assumption is that the noise and non-stimulus-locked brain activity present in the pre-stimulus period continues into the post-stimulus period, where the stimulus-evoked activity is linearly superimposed. We model the pre- and post-stimulus sensor data as:

$$y_{pre}^n = Bu_{pre}^n + v^n \quad (1)$$

$$y_{post}^n = Fx^n + Bu_{post}^n + v^n \quad (2)$$

where the number of sensors is K , the number of voxels is L , the number of inference factors is M , and the total number of time points is N . y^n is the $L \times 1$ measured electromagnetic signal vector at time $n = 1 : N$, x^n is the $L \times 1$ voxel activity vector at time $n = 1 : N$, u_{pre}^n and u_{post}^n are the $M \times 1$ pre- and post-stimulus interference factors at time $n = 1 : N$, and v^n is the $K \times 1$ sensor noise vector at time $n = 1 : N$. F is the $K \times L$ leadfield matrix and B is the $L \times M$ interference mixing matrix. Using a 2-dimensional leadfield results in the interleaving of the leadfield columns for the two directions. Likewise the number of voxel time courses is doubled to represent the two dipolar directions at every voxel. (This method can also be extended to 3 directions for use with EEG data.) The dimensions of F becomes $K \times 2L$ and the dimensions of x^n becomes $2L \times 1$. Both v^n and B are learned from the pre-stimulus period and then used in the estimation of x^n and u^n with the post-stimulus data.

The signals x , u , v are assumed to be independent zero-mean Gaussian distributions. The precision matrices for the factors u^n and then sensor noise v^n are diagonal, where u_j^n has precision 1 and v_i^n has precision λ_i . The precision matrix ν_j for each x_j^n is a 2×2 matrix that allows for correlation between the two directions of each dipole at every voxel. The entire precision matrix ν is a $2L \times 2L$ block-diagonal matrix.

The model distributions are:

$$p(y^n|x^n) = \mathcal{N}(y^n|Fx^n + Bu^n, \lambda) \quad (3)$$

$$p(x^n) = \mathcal{N}(x^n|0, \nu) \quad (4)$$

$$p(u^n) = \mathcal{N}(u^n|0, I) \quad (5)$$

$$p(v^n) = \mathcal{N}(v^n|0, \lambda) \quad (6)$$

We can redefine the notation such that: $x'^n = \begin{pmatrix} x^n \\ u_{post}^n \end{pmatrix}$, $F' = (FB)$, and $\nu' = \begin{pmatrix} \nu & 0 \\ 0 & I \end{pmatrix}$.

With this new notation, the estimation problem in the post-stimulus period reduces to:

$$y_{post}^n = F'x'^n + v^n \quad (7)$$

$$p(x'^n) = \mathcal{N}(x'^n|0, \nu') \quad (8)$$

The posterior over x'^n is Gaussian:

$$p(x'^n|y^n) = \mathcal{N}(x'^n|\bar{x}'^n, \Gamma) \quad (9)$$

where

$$\bar{x}'^n = \Gamma^{-1}F'^T\lambda y^n \quad (10)$$

$$\Gamma = F'^T\lambda F' + \nu' \quad (11)$$

The marginal log-likelihood function in this new notation is:

$$\mathcal{L} = \sum_n \log p(y^n|\nu') = \frac{N}{2} (\log|\nu'| + \log|\Gamma| - Q + \text{constant}) \quad (12)$$

where $Q = \frac{1}{N} \sum_n \bar{x}'^n \bar{x}'^{nT}$. We can derive an updates rule for ν' using an Expectation-Maximization (EM) algorithm, $\nu'^{-1} = Q$, but this algorithm has a slow convergence rate for a large number of voxels. Thus, we have derived a faster algorithm that uses a fixed point method [7]. The update rule for ν' for this method is:

$$\nu'^{-\frac{1}{2}} = S^{-\frac{1}{2}}(S^{\frac{1}{2}}QS^{\frac{1}{2}})^{\frac{1}{2}}S^{-\frac{1}{2}} \quad (13)$$

where $S = \nu'^{\frac{1}{2}}WF'\nu'^{-\frac{1}{2}}$ and $W = \Gamma^{-1}F'^T\lambda$. The source time courses are estimated from 10 are iteratively computed with ν' in the algorithm.

2.2 Functional Connectivity

We chose to employ two pair-wise connectivity metrics: coherence and imaginary coherence. Coherence is a traditional metric of connectivity and is the frequency domain representation of cross-correlation. The coherence is a complex-valued quantity; we looked at both the magnitude of the coherence and the imaginary part of the coherence alone. *Imaginary coherence* is a relatively new metric developed for use with MEG and EEG data [3]. It only reflects the coherence that is non-instantaneously mixed. Functional connectivity methods with MEG are subject to spurious correlations arising from instantaneous correlations at the sensors. While imaginary coherence under-estimates the coupling between two brain areas, it has been shown to be more robust than coherence when using MEG source reconstructions [1]. Coherence and imaginary coherence contain complimentary information. We used the coherence measure to reconstruct the correlations and imaginary coherence to determine which correlations are instantaneous or non-instantaneous.

2.3 Experimental Methods

Source Localization

We conducted tests using simulated data with realistic source configurations. The brain volume was segmented into 5mm voxels and a two orientation ($d_c = 2$) forward leadfield was calculated using a single spherical-shell model [5]. The data time courses were partitioned into a pre-stimulus period where there is only noise and interfering brain activity and a post-stimulus period where there is the same (statistically) noise and interference factors plus source activity of interest. The pre-stimulus activity consisted of the resting-state sensor recordings collected from a human subject and is presumed to have spontaneous activity (i.e., non-stimulus evoked sources) and sensor noise; this activity was on-going and continued into the post-stimulus period, where damped-sinusoidal sources were seeded and projected to the sensors through the leadfield. We were able to adjust the signal-to-noise-plus-interference ratio (SNIR), the correlations between the different voxel time-courses (inter-dipole), and the correlations between the two orientations of the dipoles (intra-dipole) to examine the algorithm performance on unknown correlated sources and dipole orientations. Champagne is compared to two commonly used source localization algorithms: minimum variance adaptive beamforming (MVAB) [6] and sLORETA [4]. We used a metric (A') that weighs hits versus false positives to assess the localization accuracy and the correlation coefficient between the seeded and estimated time-courses to assess time-course reconstruction accuracy. We also ran Champagne and MVAB on an auditory evoked field (AEF) data-set. A tone was presented to a control subject 120 times and the three algorithms were run on the stimulus-locked average of the sensor data. This data set is notoriously difficult to reconstruct due to the highly correlated dipoles in the right and left auditory cortices.

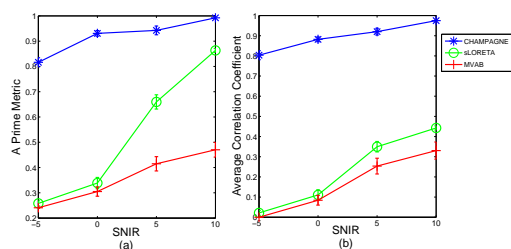


Figure 1: Performance evaluation: (a) Aggregate localization accuracy results for MVAB, sLORETA, and Champagne (CHAMP) for recovering three correlated sources with unknown orientations. (b) Estimated time-course correlation coefficient results.

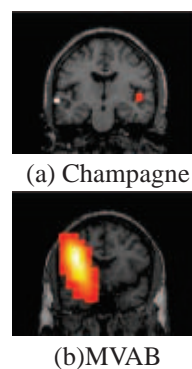


Figure 2: Performance on a real auditory data-set.

Functional Connectivity

We used simulated data to investigate Champagne’s ability to uncover interacting brain activity. For the pre-stimulus period we used Gaussian noise, instead of the real-brain noise described above. We used $SNIR = 5dB$ and an intra-dipole correlation of 0.5. The sensor data is shown in Figure 3(a). We simulated a network of 7 nodes (or voxels), where there were two networks, one left and one right, and two deep ”common source nodes”. We first localized the sources using Champagne, MVAB, and sLORETA and then assessed the connectivity from the estimated sources. The inter-dipole correlations are depicted in the diagram found in Figure 4(a) where the color of the lines between the sources denotes the strength of correlation, with red being high and blue being weak (see colorbar in Figure 4(e)). The line type indicates whether the mixing was instantaneous (dashed) or non-instantaneous (solid). The ”common source” nodes were added to simulate

the effect of instantaneous correlations on the metrics. The voxels in the left and right networks were all instantaneously coupled with the common source voxels, but coupling was a different strength.

3 Results and Discussion

Figure 1 demonstrates that Champagne outperforms MVAB and sLORETA in both location accuracy and time-course reconstruction. Figure 2 shows that Champagne is able to recover the bilateral dipoles in auditory cortex, while MVAB finds only the source on the left. The results for sLORETA are not shown, but it was also not able to localize two compact, bilateral dipoles in auditory cortex. Figure 3(b), (c), and (d) show the source reconstruction results from Champagne, MVAB, and sLORETA respectively. The white and black circles mark the true locations of the sources and the surface plot shows the maximum intensity projection of the power of the source estimate at every voxel, illustrating the inferred location of the sources. Champagne was able to resolve the network on the left even though the seeded voxel locations were relatively close to one another and the time-courses were correlated.

The functional connectivity results are depicted in Figure 4. As described above, we used the coherence measure to reconstruct the correlations (shown by the color of the lines) and imaginary coherence to determine which correlations are instantaneous or non-instantaneous (shown by dashed versus solid lines). The similarity of the ground truth (a) and Champagne (b) plots demonstrates that these two quantities can be used in conjunction to uncover the strength and lags (instantaneous vs. non-instantaneous) of interactions in a network of brain areas. The common sources are not shown to confound the connectivity results with Champagne. MVAB (c) and sLORETA (d) both show an over-estimation of the connectivity and fail to reconstruct the ground-truth connectivity. We decided to proceed with the connectivity analysis with MVAB and sLORETA regardless of the failure of these algorithms to localize the sources because it is common practice to do region-of-interest analyses.

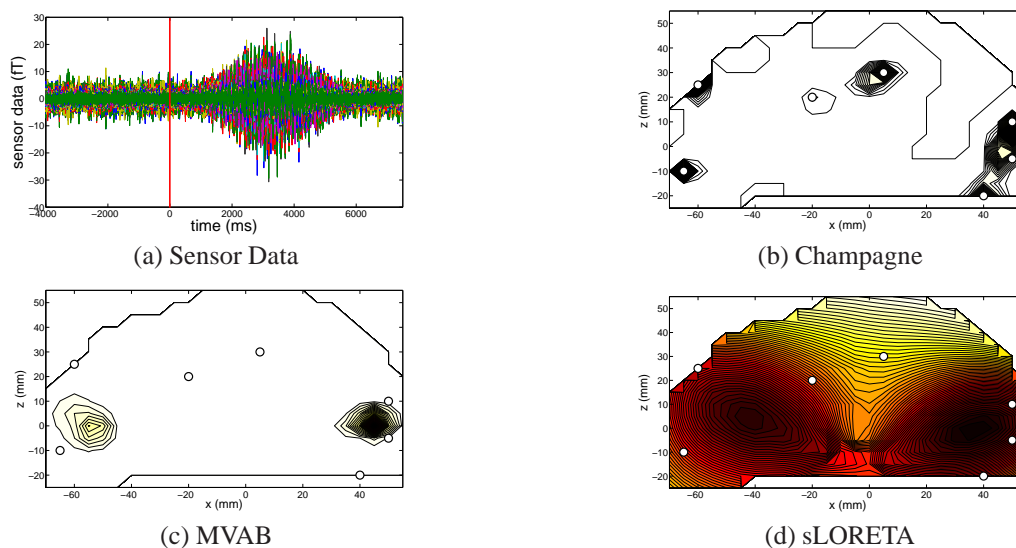


Figure 3: Source Localization: (a) Sensor data with SNIR = 5dB, the red line depicts the stimulus onset. (b) Source localization results for Champagne (c) MVAB and (d) sLORETA. The white circles show the seeded location of the sources and the surface plot shows the estimated location of the sources.

4 Conclusion

We have demonstrated that Champagne is superior in localizing correlated dipoles in the presence of noise and interfering brain activity. The sparse solution to the inverse problem obtained from Champagne is well suited for functional connectivity analyses as the number of active voxels is significantly smaller than with other techniques commonly used, such as MVAB and sLORETA. An extension of this work will be to incorporate multivariate methods of functional connectivity analyses. We have started work in this area, but the results thus far have not been as robust as those obtained with the pair-wise metrics. In addition to simulated data, we must extend our technique to real brain data. This method holds promise in improving both source localization and functional connectivity analyses in tasks that require the integration of information across a number of brain areas. We are also working to use Champagne for EEG source localization. Our preliminary results have shown that this method has the potential to improve the inverse problem solution in EEG as well.

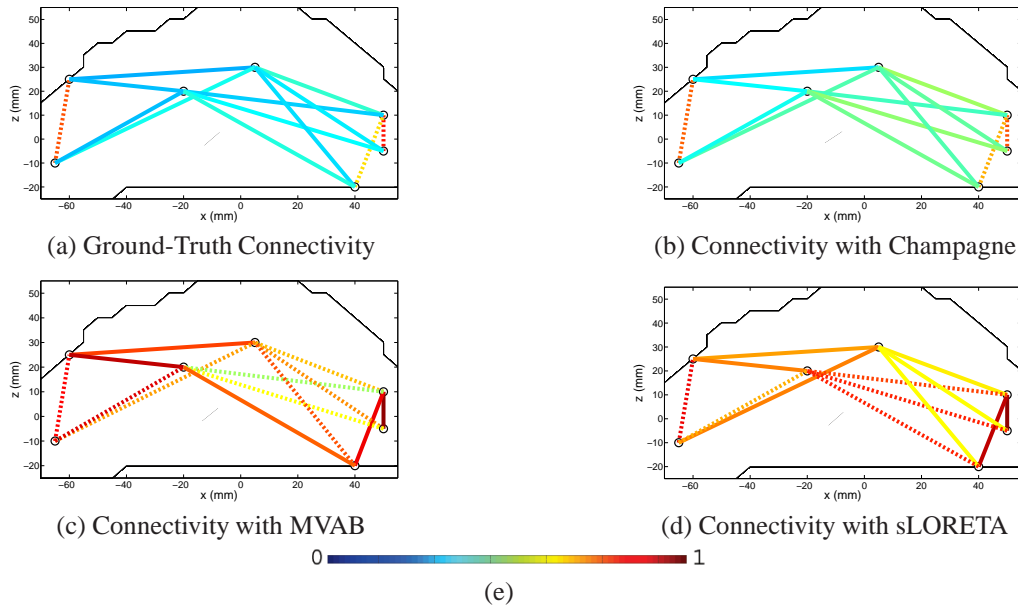


Figure 4: Functional Connectivity: (a) Ground-truth functional connectivity between sources and "common sources". Reconstructed networks using (b) Champagne, (c) MVAB and (d) sLORETA. The color (see (e)) shows the strength of coupling and the line type shows the lag of integration.(solid for instantaneous, dashed for non-instantaneous).

References

- [1] A.G. Guggisberg, et al., "Mapping functional connectivity in patients with brain lesions," *Annals of Neurology*. vol. 63 no. 2, pp. 193-203 2007.
- [2] S.S. Nagarajan, et al., "A probabilistic algorithm for robust interference suppression in bioelectromagnetic sensor data," *Stat Med*. vol. 26, no. 21, pp. 3886–910 Sept. 2007.
- [3] G. Nolte, et al. Identifying true brain interaction from EEG data using the imaginary part of coherency," *Clinical Neurophysiology*. vol. 115, no. 10, pp. 2292-307, 2004.
- [4] R.D. Pascual-Marqui, "Standardized low resolution brain electromagnetic tomography (slorete): Technical details," *Methods and Findings in Experimental and Clinical Pharmacology*, vol. 24, no. Suppl D, pp. 5–12, 2002.
- [5] J. Sarvas, "Basic mathematical and electromagnetic concepts of the biomagnetic inverse problem," *Phys. Med. Biol.*, vol. 32, pp. 11–22, 1987.
- [6] K. Sekihara and S.S. Nagarajan, "Adaptive Spatial Filters for Electromagnetic Brain Imaging," Springer; 1 edition (June 6, 2008).
- [7] D. Wipf, et al., "A Unified Bayesian Framework for MEG/EEG Source Imaging," *Neuroimage* vol. 44, no. 3, pp. 947-966, 2009.
- [8] D. Wipf, et al., "Estimating the Location and Orientation of Complex, Correlated Neural Activity using MEG," *Advances in Neural Information Processing Systems 21* 2009.
- [9] D. Wipf, et al., "Robust Bayesian Estimation of the Location, Orientation, and Timecourse of Multiple Correlated Neural Sources Using MEG," *Neuroimage In Revision*.